Journal of Science and Sustainable Development (JSSD), 2025, 13(2), 72-94

ISSN: 2304-2702 (print); 2414-4479 (online)
DOI: https://doi.org/10.20372/au.jssd.13.2.2025.0650

RESEARCH PAPER

Synergetic Effect of Ni-CuO Nanocomposites with Activated Carbon Synthesized from Zeamays Bark for the Removal of Methylene Blue Dye

Tibebu Alemu*, Teshome Abebe, Ahmed Abdurauf, Girmaye Asefa, Bulti Abdisa, Gemechis Fikadu, Kumela Dabesa, Bekele Negasa

Department of Chemistry, Ambo University, Ambo, Ethiopia

Corresponding Author:** Email: **tibebu.alemu@ambou.edu.et

Abstract

In this study, nanomaterial adsorbents including CuO, Ni-CuO, Ni-CuO/activated carbon (AC), and Ni-CuO/zeamays bark (ZB) were synthesized and evaluated for the removal of methylene blue (MB) dye from wastewater discharged by Anmol Paper Production PLC. Structural and surface characterizations were performed using X-ray diffraction (XRD), Fourier-transform infrared spectroscopy (FT-IR), scanning electron microscopy (SEM), and UV-visible spectroscopy (UV-Vis). XRD analysis confirmed the formation of a monoclinic CuO phase, with a reduction in crystal size from 34.26 nm (CuO) to 18.06 nm (Ni-CuO/ZB). SEM revealed a porous, hair-like morphology in Ni-CuO nanocomposites. FTIR spectra indicated the presence of OH and CO functional groups, enhancing adsorption potential. UV-Vis analysis showed a bandgap reduction from 3.22 eV (CuO) to 2.10 eV (Ni-CuO/AC) and 1.75 eV (Ni-CuO/ZB), suggesting improved visible light absorption. Batch adsorption experiments showed that Ni-CuO/ZB achieved the highest MB removal efficiency of 99.03% under optimized conditions: 110 ppm dye concentration, pH 12, 1.0 g adsorbent dosage, and 120 minutes contact time. The adsorption process conformed to the Freundlich isotherm model and pseudo-second-order kinetics ($R^2 = 0.99$), indicating multilayer adsorption and a chemisorption mechanism. Overall, the Ni-CuO/ZB nanocomposite demonstrated superior performance, making it a cost-effective and sustainable candidate for industrial wastewater treatment.

Keywords: Ni-CuO nanocomposites, Activated carbon, Zeamays bark, Adsorption isotherm, Methylene blue

Introduction

Industrial growth and population expansion are driving the release of significant amounts of organic and inorganic pollutants into the environment, primarily from industries such as textiles, cosmetics, paper, and leather production (Islam *et al.,* 2025). Organic dyes, such as bromophenol blue, methyl blue, methyl orange, malachite green, rhodium B, and crystal violet, are carcinogenic, mutagenic, and toxic organic chemicals (Sharma and Singh, 2021). This heavy reliance on these dyes leads to the production of contaminated water. Methylene blue dye (MB) is a popular cationic dye used in the pulp and paper industry for staining tissues and cells, as well as in medicine as an antiseptic and antifungicide (El Malti *et al*., 2024). However, MB has harmful impacts on humans, including irritation of the mouth, throat, esophagus, stomach, skin irritation, nausea vomiting, dizziness, headache, and fever (Suryowati, 2024).

Several wastewater treatment techniques have been employed, such as coagulation, photo-degradation, filtration, adsorption, and electrochemical oxidation. For example, (Kamani *et al*., 2024) investigated the degradation of Reactive Red 198 (RR198)

using NZVI nanoparticles via the Advanced Sono-Nano-Fenton hybrid method. Accordingly, the Author achieved 97% degradation efficiency within 60 minutes whereas the degradation process followed pseudo-first-order kinetics and best fitted Langmuir-Hinshelwood model (Andreucci *et al*., 2014). However, photodegradation has limitations due to the demand for specific light sources, high energy consumption, and generation of harmful byproducts (Veisi *et al.,* 2016). Adsorption presents a more attractive alternative due to its simpler operation, high efficiency in removing pollutants, eco-friendly, and cost-effective nature. TiO_2–ZnO/biochar NCs using the sol-gel method engaged for the degradation of furfural in an aqueous solution resulted in 96 % removed capacity at an optimal degradation conditions of pH 3, catalyst dosage of 1 g/L, and pollutant concentration of 10 mg/L within 15 min (Hasanzadeh *et al.,* 2023). Adsorbents such as metal oxides, activated carbon, and silica exhibit exceptional affinity and binding capacity towards dye molecules (Hasanzadeh *et al*., 2023).

Currently, commercial activated carbon (CAC) is being utilized as an adsorbent for organic materials, but its high cost, limited adsorption capacity, and slow uptake rates have led to its decline (Sharma *et al*., 2022). Agro-waste-based adsorbents are promising due to their high surface area, good recyclability, and enhanced adsorption capacity, rate, and efficiency. Maize cobs are being used as an adsorbent for pollutant removal due to their abundance and eco-friendly nature (Fu *et al*., 2022). Salix babylonica leaves powder (SBLP) has been successfully used for the removal of methylene blue (MB) from aqueous solutions through an adsorption process (Opeolu, 2009).

Previous report indicated that MB has been treated using graphene oxide adsorbent and efficient adsorption was recorded as the dye is electrostatically attracted toward the negatively charged adsorbent. Adsorbents like AC, GO, and CNTs have been effectively employed for the removal of MB, demonstrating impressive adsorption capacities of 270.27 mg/g, 243.90 mg/g, and 188.68 mg/g, respectively (Luong *et al*., 2024). Besides to the above studies, nano-adsorbents were successfully utilized for the treatment of heavy metal (Cu^{2+}) using GO nanosheets modified with Fe_3O_4 nanoparticles. It is supposed that nanoparticles likely create additional pores within the graphene structure, enhancing its ability to adsorb pollutants. This increased porosity improves access to pollutants, promotes their diffusion into the material, and shortens the diffusion path (Matandabuzo, 2016). Similarly, (Rashed *et al*., 2017) prepared TiO_2 nanoparticle coated with sewage sludge-based AC (ASS) and tested for simultaneous adsorption of methyl orange dye (MO) and Cd^{2+} ions. It was found that high treatment efficiency of MO dye and Cd^{2+} were achieved with TiO_2/AC. In their finding, the adsorption of TiO_2/ASS NC led to significantly faster and higher degradation of MO compared to ASS alone (74.14% vs. 94.28% removal efficiency at pH 7). Despite the previously reported results apparently promising, the efficiency and cost effectiveness of the adsorbents for pollutants removals with the aid of NC remains unsatisfactory. Therefore, developing more efficient, simple, and cost-effective adsorption techniques is crucial for environmental remediation (Rashed *et al*., 2017).

Therefore, this study intended to explore adsorption techniques using Ni doped CuO nanomaterials modified AC for effective treatment of wastewater containing MB dye discharged from Anmol paper products PLC (Ginchi, Ethiopia). As this industry uses different coloring agents in particular MB, it is found discharging effluents to the environment without pretreatment. Recently, (Alemu *et al.,* 2024) investigated the wastewater treatment discharged from the same site using photodegradation technique. Ag-CdO/PANI NC was employed and the most effective photodegradation of BPB dye in the wastewater samples is achieved 98.64% at pH 8, 0.16 g of catalyst dose and 180 min light irradiation time which agree with the finding of (Lakkaboyana *et al*., 2019). Taking the drawback of photodegradation methods into consideration, the researchers have applied the adsorption method to remove organic pollutant (in particular MB) from Anmol Paper Product PLC

with the aid of nanostructured materials since they possess sufficient surface area and easy tailoring of surface properties. Furthermore, surface modification of nanomaterials with activated carbon derived from zeamays bark was carried in order to enhance the activity of adsorbents (Alemu *et al.*, 2022).

ZB stands out as a promising material for adsorption due to its non-toxic, readily available and highly porous structure (Igwegbe *et al*., 2021). Copper oxide nanoparticles (CuO NPs) are a perfect complement due to their well-understood surface chemistry, which can be customized through doping techniques. Additionally, their narrow band gap makes them ideal for applications involving both light activation (photoconduction) and adsorption. To improve the adsorption capacity of CuO nanostructures for pollutant removal, the research have strategically introduced nickel (Ni) as a dopant so as to effectively tailor its band gap, resulting in Ni-CuO NCs with enhanced capabilities for removing MB from wastewater (Chowdhury et al., 2021). This approach resulted in Ni-CuO NCs with enhanced capabilities for removing MB from wastewater. A comprehensive literature review indicates that there is lack of research investigating Ni-CuO NCs modified with agro-waste-based activated carbon for the targeted removal of organic pollutants present in the wastewater stream generated by Anmol Paper Product PLC (Shah *et al*., 2020).

The research aims to develop a novel adsorbent, Ni-doped CuO NPs modified with AC from locally available resources, for treating wastewater containing MB pollutant of MB pollutant containing wastewater discharged by Anmol Paper Products PLC. Advanced characterization tools like XRD, SEM, FTIR, and UV-Vis spectroscopy were used to analyze the material's structure, morphology, functional groups, and band gap. The optimal conditions for pollutant adsorption were also being investigated.

Materials and Methods

Experimental Sites

Zeamays Bark (ZB) was collected from Jibat District, Oromia Region, Ethiopia. The synthesis of CuO NP, Ni-CuO NC, Ni-CuO/AC NC, and Ni-CuO/ZB NC, preparation of activated carbon (AC) from ZB, optical properties was analyzed using UV-Vis spectrophotometer, batch adsorption experiments and optimization were conducted at Ambo University, Chemistry Research Laboratory. The elucidation of functional group has been conducted at Addis Ababa Science and Technology University, the measurement of crystalline structure and morphology were done at Adama Science and Technology University, Ethiopia.

Apparatus and Instruments

The UV-Vis spectrophotometers (UV-Vis, Sunny ultraviolet-visible spectrophotometer, model Uv-7804C Print), Fourier-transform infrared (FTIR, JASCO FT/IR-6700), scanning electro-microscope (SEM, JCM-6000 PLUS Bench Top SEM, JEOL, and Japan) and x-ray diffraction (XRD, D2, Phaser, Bruker) are instruments used in this research work. Microplant grinding machine (NM-8300, Nima, 220x80mm, Japan), filter paper (Whatman 41), plastic funnel, graduated cylinder, electronic analytical balance (A160, Denver), magnetic starrier (Model № 690/21), centrifuge (Model 80-2, China), refrigerator (MRF451), pH meter (CPI501), drying Oven (DHG-9070A), muffle furnace (PYRO THERM FURNACES, SLAB12/5) and common laboratory apparatus were used in this study.

Chemicals and Reagents

The AC prepared from ZB was used as adsorbent and wastewater containing MB dye is employed as adsorbate. Analytical grade (AG) chemicals/reagents such as sulfuric acid (H_2SO_4, UNI CHEM, 98%), nitric acid (HNO_3 , LOBA CHEM, ACS, 69-70%), potassium hydroxide (KOH, AR, ≥85%), sodium hydroxide (NaOH, AR, 99.8%), hydrochloric acid (HCl, LOBA CHEM PLC, 35%), hydrogen peroxide (H_2O_2, UNI CHEM, 30%), nickel nitrate monohydrate ($Ni(NO_3)_2.H_2O$, UNI CHEM, 98%), copper chloride dehydrate

($CuCl_2.2H_2O$, UNI-CHEM CAS, 99.5%), and ethanol (CH_3CH_2OH, Alpha Chemika, AE754, 95%) are chemicals used to prepare pristine and modified CuO based NP and NC.

Collection of Wastewater Sample

Wastewater sample was collected from Anmol Paper Products PLC (Ginchi, Ethiopia) in March 2023 following US-EPA sampling guideline (US-EPA, 2009). Anmol Paper Products PLC is one of the paper production plant located in Ginchi Town, Dendi Woreda (IFPRI, 2012), West Shoa Zone, Oromia Regional State, Ethiopia. Though it produces high quality papers, Anmol Paper Products PLC release organic pollutants to the environment without pretreatment (Alemu *et al.*, 2024). The wastewater sample contains MB was collected in triplicate (n = 3) into 1 L volume glass container. The samples were stored in an ice-cooled box, promptly transported to the Chemistry Research Laboratory, and kept at 4 °C until the adsorption experiments were carried out.

Collection of ZB and Preparation of AC

The collected ZB has been washed with DI water to get rid of unnecessary impurities. Then, it was exposed to sunlight for several days and dried in oven at 105 ^{o}C, milled by Microplant Grinding machine till the size of ZB is 1 mm and finally sieved. It was activated by carbonization process in furnace at 400 ^{0}C for 2 hr. The activated material was cooled for few a minute and kept in desiccators (Matandabuzo, 2016).

Synthesis of CuO NP

CuO NP was prepared through a co-precipitation method. In this process, 15 g of $CuCl_2.2H_2O$ was taken and dissolved in 50 mL DI water. The mixture was then stirred for 1 hr using magnetic stirrer. 20 mL NaOH was added to the above solution and kept for 1 day to form the gel. The gel was filtered and dried at 110 °C in oven followed by calcinations at 400 °C for 2 hr. The black colored material was formed indicating the formation of CuO NP (Satari et al., 2021).

Synthesis of Ni-CuO NC

In a typical synthesis procedure, a stoichiometric amounts of 5 g Ni $(NO_3)_2.3H_2O$ and 15 g $CuCl_2.2H_2O$ was dissolved in DI water. The mixture was stirred at temperature of 80 °C till the gel was formed. The formed gel is washed 2-3 times with CH_3CH_2OH in order to avoid any contaminations. Subsequently, the cleaned and dense precipitate was formed and heated at 110 °C for 1 hr in oven. Finally, it was grinded and calcinated at 400 °C for 2 hrs while the crystalline phase of Ni-CuO NC was achieved (Xie *et al.,* 2020).

Synthesis of Ni-CuO/AC NC and Ni-CuO/ZB NC

5 g of as-synthesized Ni-CuO NC was added to 250 mL volumetric flask to which each 10 g of AC and ZB was added. Ni-CuO NC was mixed with AC and ZB upon stirring at 200 rpm for 3 hr at 60 ˚C. Then, Ni-CuO NC was homogenized with AC and ZB, followed by filtration and washing by DI water. After drying at 70 ˚C for 24 hr the Ni-CuO/AC and Ni-CuO/ZB NC were formed and kept in dissector (Chesman *et al.,* 2013).

Characterization

The FT-IR was employed to reveal the chemical environment of CuO NP, Ni-CuO NC, Ni-CuO/AC NC and Ni-CuO/ZB NC via scanning the sample between 4000 to 400 cm^{-1} (Hi, 2021). Morphology of as-synthesized materials were investigated using SEM (Yang and Yang, 2018). It was scanned by 10 kV on 20 μm electron beam at X1500 magnification power. XRD was measured between 10 - 80 in order to determine crystal structure of as-synthesized nanomaterials. The crystalline size of the adsorbents were calculated as in follow (Sukumar *et al*., 2020).

$$D = \frac{k\lambda}{\beta \cos \theta} \quad \text{.....1}$$

Where D represent the average particle size, *k* - Scherrer constant (0.9), λ - wavelength (0.15406 nm), B - full width at half-maximum (FWHM) in radians, and θ - diffraction angle.

UV-Vis spectrometry was also used to investigate the optical characteristics of adsorbents between 200 to 800 nm (Khan *et al*., 2022). The band-gap energy was calculated using eq. 2 below:

$$E_g = \frac{hc}{\lambda_{max}} eV \quad \text{.....2}$$

Where h - Planck's constant, c - speed of light, λ - cut off wavelength and E_g - optical band gap (Gomathi *et al*., 2016).

The organic contaminant percentage removal efficiency from wastewater sample can be determined as indicated in eq.3 below:

$$\%R = \frac{c_o - c_e}{c_o} \times 100 \quad \text{.....3}$$

Where R - removal rate, C_o and C_e - liquid-phase concentrations of adsorbate (mg L^{-1}) at initial and equilibrium position, respectively (Al Ani and Al Amri, 2015).

Study of Operational Parameters

Effect of initial concentration of MB in wastewater: In this study, the initial concentration of wastewater containing MB was determined using calibration curve and after determined, the actual concentration was varied from 80 to 120 ppm in adsorption time of 0-120 min, pH 12 and 0.8 g adsorbent dose. The absorbance values of the dyes were recorded at λ_{max} (Medhat *et al*., 2021).

Effect of irradiation time: The effect of irradiation time on decolourization of wastewater sample was studied at contact time of 0, 20, 40, 60, 80, 100 and 120 min. using 0.8 g of the adsorbents load, pH 12 and 110 ppm concentration of wastewater sample.

Effect of adsorbent dosage: the adsorbent dosage of 0.20, 0.40, 0.60, 0.80 and 1.00 g was taken and added to 110 ppm wastewater sample while pH solution was adjusted to 12 and adsorption was undertaken for 120 min.

Effect of pH: 110 ppm concentration of MB containing wastewater with pH value fixed to 2, 4, 6, 8, 10 and 12 were prepared using 0.80 g adsorbent doze and adsorption lasts for 120 min.

Adsorption of Wastewater Sample

The adsorption was conducted by taking 80 to 120 ppm concentration of MB containing sample, 2 to 12 pH of the solution, 0.20 to 1.00 g of adsorbents conducted for 120 min at 25 °C. The amount of dye adsorbed to the unit weight of adsorbent at equilibrium and time t was evaluated (Raut *et al*., 2021):

$$q_t = v\frac{(c_o - c_t)}{m} \quad \text{.....4}$$

Where, q_t - amounts adsorbed (mg/g) at time t, C_t - concentration of MB in the sample (mg/L) at time t; V - volume of the sample (L) and m - dry weight of adsorbent (g).

Langmuir Isotherm

The Langmuir adsorption isotherm follows the principles of forming monolayer at adsorbent surface and determined as follow (Shahmohammadi-Kalalagh *et al*., 2011).

$$\frac{C_e}{q_t} = \frac{1}{K_L q_{max}} + \frac{C_e}{q_{max}} \quad \text{.....5}$$

Where q_e - amount of adsorbed MB (mg/g) at equilibrium, C_e - equilibrium concentration (mg/L) of MB, q_{max} - monolayer adsorption capacity (mg/g) and K_L - Langmuir adsorption constant and measure the adsorption affinity of organic pollutant to adsorbent active sites.

Freundlich Isotherm

This adsorption isotherm follows the principles of forming layers at heterogeneous surface and is commonly determined as (Ayawei *et al*., 2017):

$$\log q_e = \log K_f + \frac{1}{n}\log C_e \quad \text{.....6}$$

Where, q_e - amount of MB adsorbed at equilibrium (mg/g), C_e - equilibrium concentration of dye in sample (mg/L) and K_f and n - Freundlich isotherm constants incorporating factors affecting adsorption capacity and intensity of adsorption, respectively.

Adsorption kinetics

Pseudo first-Order Kinetics

This kinetic model is used to describe adsorption of wastewater sample as follow (Hii, 2021):

$$\ln(q_e - q_t) = \ln q_e - \ln k_1 t \quad \text{.....7}$$

Where q_e and q_t (mg/g) - amounts of adsorbate adsorbed at equilibrium and time, t respectively and k_1 - adsorption rate constant.

Pseudo Second-Order Kinetics

The pseudo second-order kinetic model can be determined as follow (Ersali *et al.*, 2013):

$$\frac{dq_t}{d_t} = k_2 (q_e - q_t)^2 \quad \text{.....8}$$

Where, k_2 - rate constant ($gmg^{-1}.min^{-1}$) for pseudo second-order adsorption and q_e - equilibrium adsorption capacity (mg/g).

Re-usability of Adsorbent

The Ni-CuO/ZB adsorbent was confirmed as the best adsorbent and the adsorption experiment was studied once the adsorbent is dried at 60 ºC in oven its re-usability tests (the overall activities are designed as shown in Fig. 1. After drying the catalyst; the adsorbent was collected, measured and prepared for the consecutive five experimental cycles. In this test followed the optimum operating conditions of 110 ppm initial concentration of wastewater sample, 0.80 g of adsorbent dose, pH 12 and 120 min contact time **(**Sravanthi *et al.*, 2016**).**

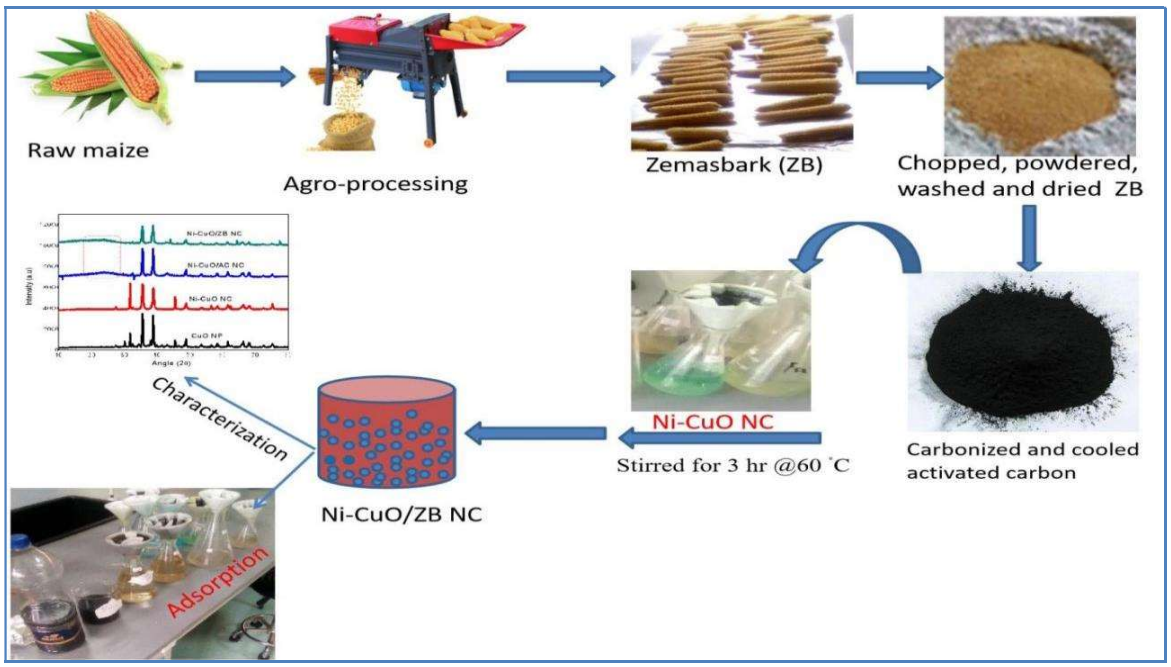

Figure 1. Schematic representation of Ni-CuO/ZB NC preparation, characterization and adsorption activities

Results and Discussions

Characterizations of As-Synthesized Nanomaterials

Analysis of surface morphology: The SEM analysis revealed distinct morphologies for the as-synthesized nanomaterials. Accordingly, Fig. 2(A), shows the crystalline and aggregated structures, suggesting a tightly packed arrangement of CuO NP. Fig. 2(B), reveals an interconnected particle with varying shapes and sizes which indicate the successful Ni incorporation into the CuO lattice, potentially disrupting the original crystal structure. On the other hand, shiny and uniformly distributed small particles compared to CuO and Ni-CuO in Fig. 2(C), suggests the effective anchoring of Ni-CuO nanoparticles onto the AC substrate (Robertson et al., 2010). In Fig. 2(D), a network of pores and hair-like structures with smaller particle sizes and a higher surface area have been observed. This implies that the successful embedding of ZB within the metal oxide structure, lead to the formation of numerous porous cavities and a reduction in particle size. Notably, the interconnected with hair-like structures suggest potentially novel properties for this particular nanocomposite. Such a distribution of particles and the presence of an interconnected, hair-like nanostructure could impart unique properties to this particular nanocomposite (NC) (Morsy *et al*., 2019).

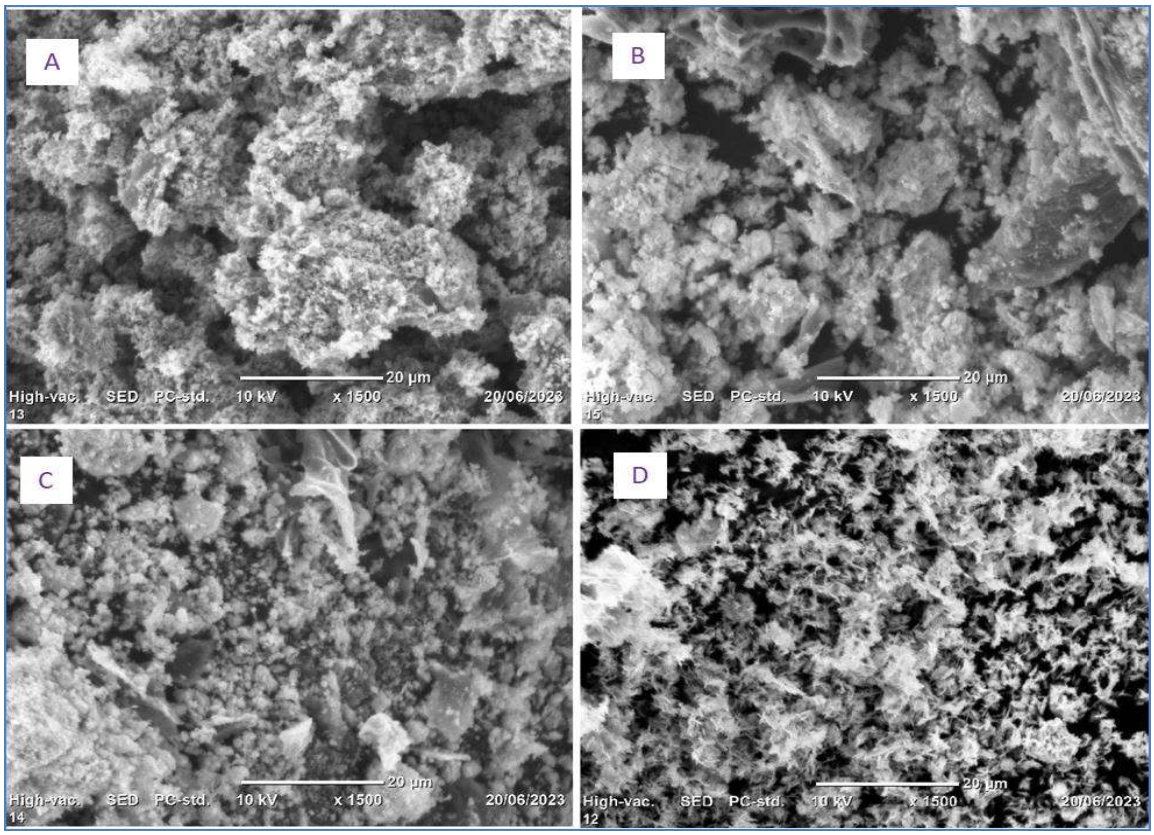

Figure 2. SEM image of (A) CuO NP, (B) Ni-CuO NC, (C) Ni-CuO/AC NC, (D) Ni-CuO/ZB NC

Study of functional group: Fig. 3, presents the FTIR spectra of CuO NP, Ni-CuO NCs, and NC modified with CAC and ZB. The spectra reveal distinct absorption peaks for CuO NP at 486.20, 596.85 and 878.90cm^{-1} correspond to the characteristic stretching vibrations of the Cu-O bond. This confirms the successful formation of CuO NP in the initial material (Suteu *et al*., 2011). Spectral analysis revealed distinctive absorption bands at 534.17, 816.21,

1380.30, and 3309.57 cm^{-1} in the Ni-CuO nanocomposite (NC). The first two peaks represent the stretching vibrations of Cu-O and Ni-O bonds in the copper oxide structure while the latter two peaks indicate the presence of OH groups, likely due to surface adsorbed water molecules or residual hydroxyl groups from the precursor materials (Suteu *et al*., 2011). This characterization tool also provided a unique fingerprint for Ni-CuO/AC NC. For instance, the peaks around 596 and 784 cm^{-1} denoted the Cu-O bonds, possibly influenced by the incorporation of Ni metal. Similarly, other peaks provide insights into the vibration of C-O-C in the AC component, Cu-O-H bending vibrations, and O-H associated with both Ni and AC. In essence, the FTIR analysis offers a detailed picture of the chemical environment within the NC, supposed the integration of Ni-CuO with AC (Al-Amri *et al*., 2015). The near-identical absorption peaks between Ni-CuO/ZB and Ni-CuO/AC suggest a close resemblance in their chemical makeup, with only minor intensity variations. This strongly indicates successful anchoring of the Ni-CuO NC onto the ZB surface. Interestingly, a small, distinct peak appears at 1004.24 cm^{-1} in the ZB spectrum, potentially attributable to in-plane deformation of aromatic C-H bonds and C-O stretching vibrations within the ZB structure itself. The peak at 1400 cm^{-1} indicated aromatic rings likely from the organic precursor. Additionally, the broad peaks between 2900 -3400 cm^{-1}, suggested the presence of both aliphatic C-H bonds and O-H groups from water molecules or surface hydroxyls. Importantly, these results confirmed the presence of metal-oxygen (M-O) bonds, possibly from CuO and Ni-CuO, within the NC structure. Even more significant, the FTIR analysis highlighted the abundance of functional groups such as O-H, C-O, C=C, C-H, C-O-C, Ni-O, Cu-O, and potentially Ni-O-Cu bonds, act as potential binding sites for organic dye molecules during the adsorption process in Ni-CuO/AC and Ni-CuO/ZB NC (Shah *et al*., 2020).

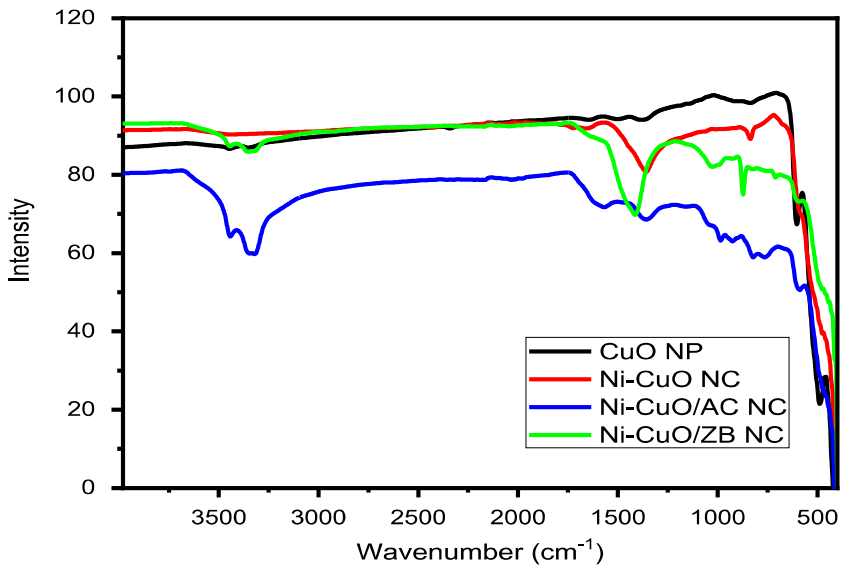

Figure 3. FTIR spectra of CuO NP, Ni-CuO NC, Ni-CuO/AC NC and Ni-CuO/ZB NC

Determination of crystal structure: Fig. 4, represents the XRD pattern of CuO NP, Ni-CuO NC, Ni-CuO/AC NC and Ni-CuO/ZB NC. The peak position for CuO NP generated at 2θ (unit of degree) = 32.02, 35.60, 38.82, 45.49, 48.73, 53.01, 58.311, 61.55, 66.30, 68.03, 72.40 and 75.30^0 correspond to (110), (-111), (111), (200), (-202), (020), (202), (-113), (-311),

(220), (311), and (004) planes, respectively. These diffraction peaks are confirmed the formation of the monoclinic CuO phase which agrees the pattern with standard JCPDS card no. 05-0661. Interestingly, the peaks observed in the analysis don't show any major shifts in position. They are also relatively sharp and intense. This suggests a high degree of crystallinity in the as-synthesized nanomaterials. Furthermore, the peak intensities corresponds to (110), (-111) and (111) are so strong as compared to the others which signifies a favorable orientation of nanoparticles along these directions. The XRD analysis did not identify any separate peaks corresponding to metallic Ni in the Ni-CuO NC. However, the existing peaks became more intense, suggesting that Ni atoms have likely replaced Cu sites within the crystal structure of the pure CuO NP, without causing a significant change in the overall crystal structure. However, the XRD peaks are observed at 35.55, 38.78, 43.20, 48.73, 61.53, 66.11, 68.01 and 75.27^0 are assigned to (-111), (111), (200), (-202), (202), (-113), (-311) and (004) planes for Ni-CuO/AC NC. The X-ray diffraction (XRD) patterns of both Ni-CuO/AC and Ni-CuO/ZB NCs displayed a series of diffraction peaks at similar angles. These peaks are characteristic of the well-established monoclinic crystal structure typically observed in CuO-based nanomaterials. However, a notable difference emerged. Both NCs exhibited an additional weak peak at 2θ values of 23.52 and 43.00 degrees. This suggests the presence of an amorphous phase, potentially arising from the AC substrate. This is due to the fact that Ac is known by its components such as cellulose, hemicellulose, and lignin which are inherently amorphous.

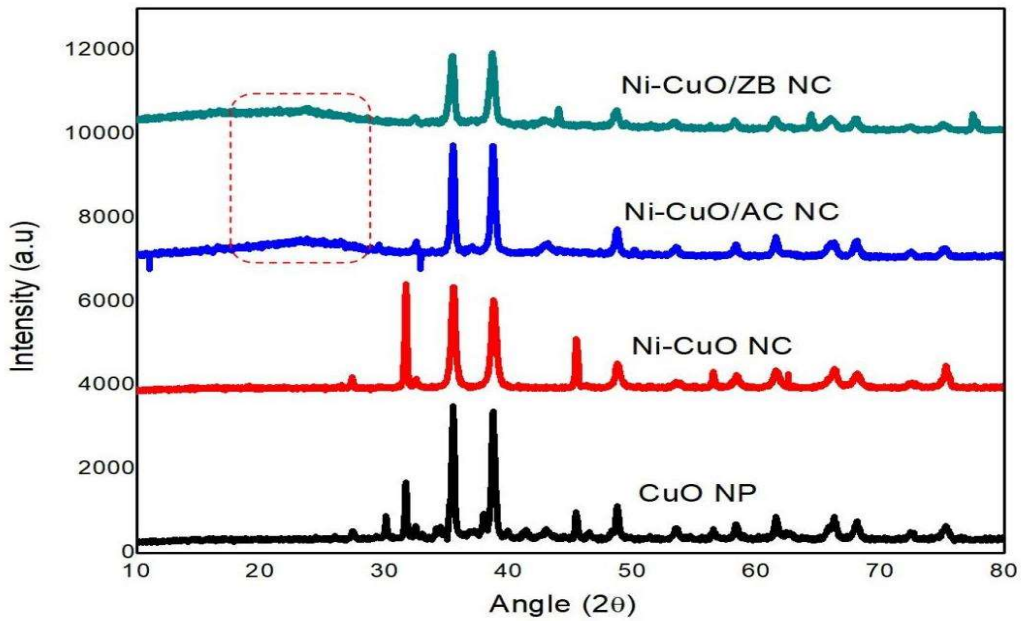

Figure 4. XRD patterns of CuO NP, Ni-CuO NC, Ni-CuO/AC NC and Ni-CuO/ZB NC

This finding aligns with the standard reference pattern (JCPDS 5-667) for AC. Eq. 1 was used to calculate the average crystallite size of the synthesized nanomaterials and the results are summarized in Table 1. Interestingly, the average crystallite size of pristine CuO has progressively decreased from 34.26 nm to 26.09, 22.46 and 18.06 nm corresponding to the sizes of Ni-CuO, Ni-CuO/AC, and Ni-CuO/ZB NC, respectively.

Table 1. Calculated crystallite sizes for as-synthesized nanomaterials

Adsorbent	**2θ**	**θ**	**Cosθ**	**FWMH**	**in rad**	**size/nm**	**Aver/nm**
CuO NP	35.6	17.8	0.9523	0.2956	0.005	30.25	34.26
	38.82	19.41	0.9433	0.2969	0.005	30.4	
	31.92	15.96	0.9619	0.2101	0.0036	42.14	
Ni-CuO NC	31.73	15.87	0.9618	0.4059	0.0069	21.81	26.09
	35.55	17.78	0.9522	0.3847	0.00654	23.25	
	38.78	19.39	0.9431	0.2718	0.0046	33.22	
Ni-CuO/AC NC	38.78	19.39	0.9433	0.3638	0.00618	24.81	22.46
	35.55	17.78	0.9523	0.3449	0.0059	25.93	
	48.73	24.37	0.9109	0.562	0.0096	16.63	
Ni-CuO/ZB NC	38.8	19.4	0.9435	0.5096	0.0087	17.71	18.06
	35.55	17.78	0.9525	0.5101	0.0087	17.53	
	43.38	21.69	0.9112	0.4937	0.0084	18.93	

Analysis of Absorption Spectral: Fig. 5, illustrates the UV-Vis spectra of the synthesized nanomaterials. Eqn. 2 is used to calculate their energy band gaps (Eg). As the materials are modified to get multi-component systems, the maximum absorption wavelength increased. As a result the maximum absorption is observed at 385, 485, 590 and 710 nm corresponding to 3.22, 2.55, 2.10 and 1.75 eV for CuO NP, Ni-CuO NC, Ni-CuO/AC NC and Ni-CuO/ZB NC, respectively (Table 2).

Interestingly, the calculated band gaps decreased significantly compared to the theoretical value for CuO NP (3.9 eV). This trend suggests that incorporating Ni and the additional materials (AC and ZB) successfully modified the electronic structure and particle size of the nanocomposites *(Chandrasekar et al.*, 2022). Moreover, treatment with ZB make the NC more effective in transforming the surface properties as compared to the NC consisting AC (Dwivedi *et al.*, 2021). The Ni-CuO/ZB NC exhibited with the peak wavelength increasing from 590 nm to 710 nm contributing to narrowing Eg to 1.75 eV. This reduction in Eg is likely due to a synergistic effect of novel metal as well as agro-waste surface modifier and ultimately enhanced the pollutant adsorption.

Table 2. Absorbance at maximum wavelength and optical band gap energy of CuO NP, Ni-CuO NC, Ni-CuO/AC NC, Ni-CuO/ZB NC

Samples	Absorbance (a.u)	λmax (nm)	Eg (eV)
CuO	0.002	385	3.22
Ni-CuO	0.04	485	2.55
Ni-CuO/AC	0.583	590	2.1
Ni-CuO/ZB	0.704	710	1.75

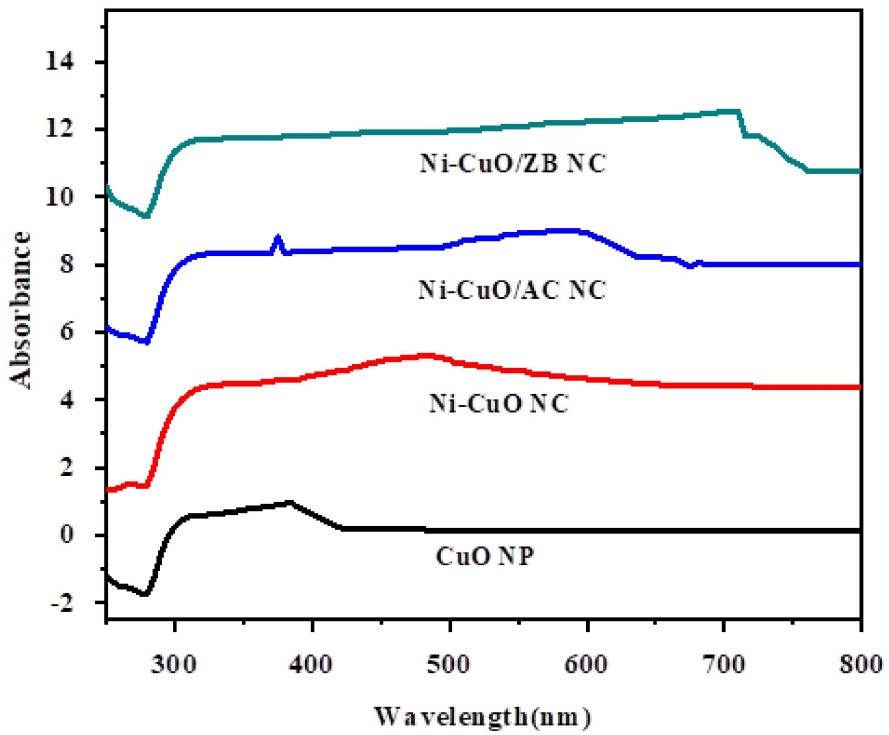

Figure 5. Absorption spectra of CuO NP, Ni-CuO NC, Ni-CuO/AC NC and Ni-CuO/ZB NC

Determination of MB Dye in Wastewater

The concentration of MB in the wastewater from Anmol Paper Product PLC was determined using a standard calibration curve. This involved measuring the absorbance of standard MB solutions at a specific maximum wavelength (665 nm) and plotting it against its known concentrations as indicated in the data summarized in Table 3. Fig. 6 shows a good linear relationship ($R^2 > 0.9661$) between absorbance and concentration within the tested range of 80-120 ppm. Using the established linear equation ($y = 0.002x - 0.133$) and the measured absorbance value of the wastewater sample (0.058), the MB concentration was calculated to be 95.5 ppm ± 0.01 ppm. The physicochemical variables of MB in wastewater samples such as pH, dissolved oxygen and its color were determined and

found as 6.67 ± 0.21, 1.10 ± 0.08 mg/L and yellow, respectively (Alemu *et al.*, 2024). The wastewater exhibited a slightly acidic nature (pH below 7), potentially due to the presence of a high organic matter load. Analysis using a calibration curve revealed a mean concentration of MB was 95.5 ± 0.01 ppm.

Table 3. The standard concentration of MBD and corresponding absorbance

	Standard concentration of MBD (ppm)				
Standard Series	80	90	100	110	120
Absorbance (λ_{max} = 665 nm)	0.033	0.038	0.072	0.089	0.108

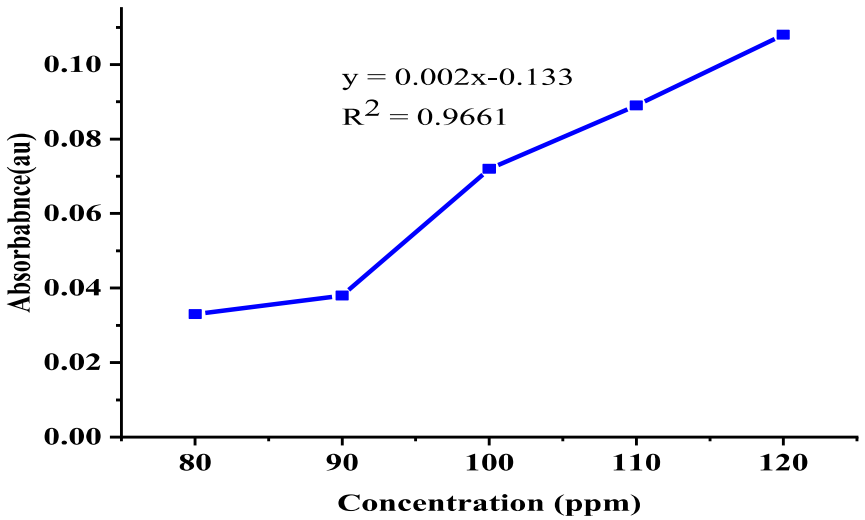

Figure 6. The calibration curve sketched using standard concentrations of MBD (80–120 ppm)

Study of Adsorption Operational Parameters

Effect of adsorbents: The batch adsorption was performed for the removal of MB from wastewater effluent fixing contact time to 120 min, concentration of MB to 80 ppm, adsorbent dose to 0.80 gm, and pH of solution to 12 (Fig. 7). Ni-CuO/ZB NC demonstrated a clear advantage in its initial adsorption rate for MB compared to other adsorbents. This is evident from the sharp rise in the adsorption curve at the beginning of adsorption experiment which can be attributed to the abundant surface area of the Ni-CuO/ZB NC. This adsorbent provide large surface area with greater number of accessible active sites which attract MB molecules at the initial adsorption process (Chakraborty *et al.*, 2020). Smaller particles and a narrower band gap appear to be contributing factors to the faster adsorption rate. The Ni-CuO/ZB nanocomposite (NC) with the smallest crystallite size (18.06 nm) and narrowest band gap (1.75 eV) exhibited a continuously increasing adsorption rate. Impressively, this NC achieved a maximum adsorption efficiency of 99.50% within just 40 minutes. Due to this exceptional performance, the Ni-CuO/ZB NC was chosen as the best adsorbent for further experiments (Juma *et al.*, 2017).

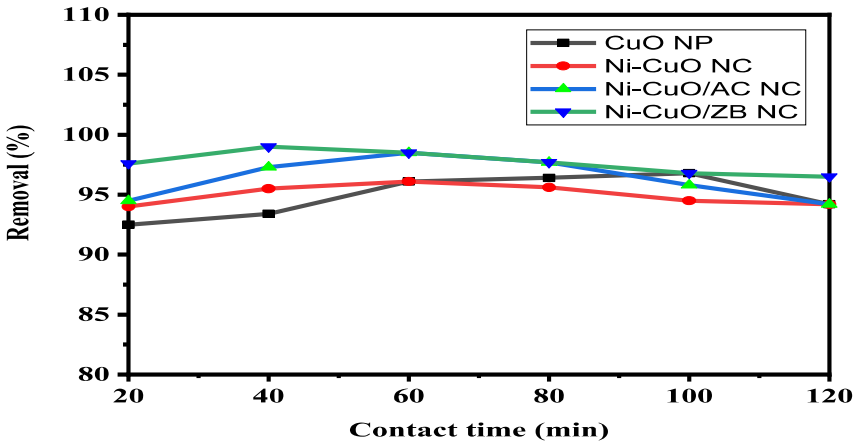

Figure 7. Effect of nature of adsorbent for adsorption of MB from wastewater sample

Effect of MB concentration in wastewater sample: This study examined the effect of initial MB concentration on its removal from wastewater using the Ni-CuO/ZB NC adsorbent. The experiment evaluated MB concentrations ranging from 80 to 120 ppm with a fixed adsorbent dose (0.8 g), pH (12), adsorption time (120 minutes), and room temperature. As shown in Fig. 8, the highest removal efficiency has been recorded at 110 ppm initial concentration of MB and taken as an optimal range for efficient adsorption. The adsorption process was rapid at initial, time and reaching its maximum removal capacity within 120 minutes for all tested MB concentrations (Mousavi *et al.*, 2022). The adsorption efficiency of Ni-CuO/ZB NC was significantly increased with contact time till it reach 120 min (98.98%) which ascribed to the availability of adsorption active sites. This high removal rate and the optimal concentration likely occur because the Ni-CuO/ZB NC has a large number of available and accessible active sites for MB dye adsorption. Regardless of initial concentration, the adsorption rate has initially fast as the positively charged MB is binded to negatively charged adsorbent surface (pH is in alkaline media). These sites become progressively occupied, leading to a steady removal tendency for all concentrations. However, resulted in a slowing down adsorption rate with increasing time as a result of surface saturation (Salih *et al.*, 2022).

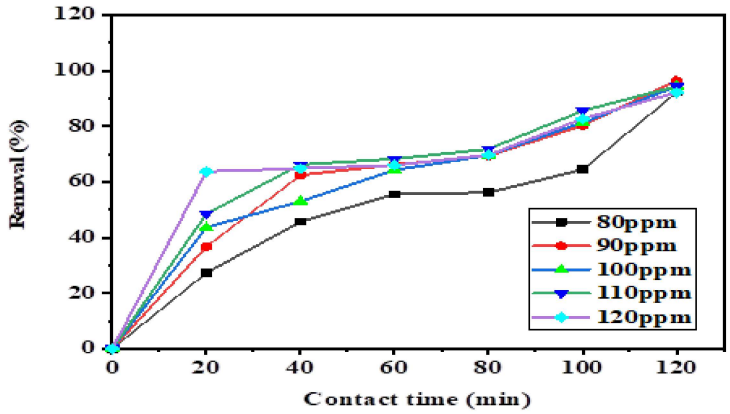

Figure 8. The effects of initial concentration of MB containing wastewater at Ni-CuO/ZB NC surface

Effect of pH: Fig. 9, indicates the adsorption of MB pollutant at Ni-CuO/ZB NC surface via varying pH value from 2 to 12 keeping the adsorbent dose at 0.8 g, dye concentration at 110 ppm and contact time at 120 min. This study revealed that the Ni-CuO/ZB NC is effective at removing MB dye from wastewater samples at various pH levels. Interestingly, the highest removal efficiency (~99%) was achieved at a pH 12. It suggests that the NC's adsorption capacity of MB is strongest when its surface is alkaline (negatively charged). This creates a favorable environment for attracting cationic pollutants (MB), through electrostatic interactions. In contrast, research shows that removing other pollutants, like methyl orange (MO) dye, using agro-waste-based adsorbents is most effective in acidic environments (around pH 4-5) signifying that under acidic conditions, the adsorbent surface becomes positively charged, while MO molecules remain negatively charged. These oppositely charged ions attract each other and enhance adsorption process. However, as the pH increases, the positive charge on the adsorbent weakens, and an abundance of OH^- in the solution repels the negatively charged MO molecules which then reduce its adsorption in basic environments (Tigrine *et al*., 2024).

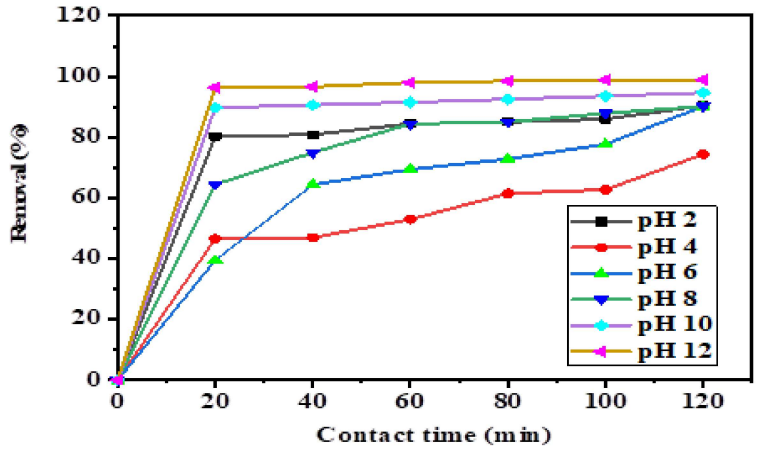

Figure 9. The effect of pH on adsorption efficiency of MBD in wastewater effluent

The effect of adsorbent load: This study investigate the extent of Ni-CuO/ZB NC in removing MB dye from wastewater using different amounts of the nanomaterial vary from 0.07 to 1.00 g while keeping other conditions constant (pH 12, MB concentration 110 ppm, contact time 120 minutes). The study revealed that 1.00 gram of Ni-CuO/ZB NCs was the most effective for removing MB (Fig. 10). This is because a higher amount of adsorbent provides more active sites, which are like tiny hooks that grab and hold onto the dye molecules. As the amount of adsorbent increases, so does the removal efficiency of the MB dye (Bedmohata *et al.*, 2015)**.** Thus, the removal capacity corresponding to 0.20, 0.40, 0.60, 0.80, and 1.00 g of Ni-CuO/ZB NC are 52.54, 49.20, 55.20, 60.48, 86.72 and 98.98%, respectively. Generally, the adsorption experiment for the treatment of MB pollutant using Ni-CuO/ZB NC adsorbent signifies the optimum removal efficiency was retained at adsorbent dose of 1.00 g, pH 12, 110 ppm concentration and 120 min contact time with removal capacity of 99.04%.

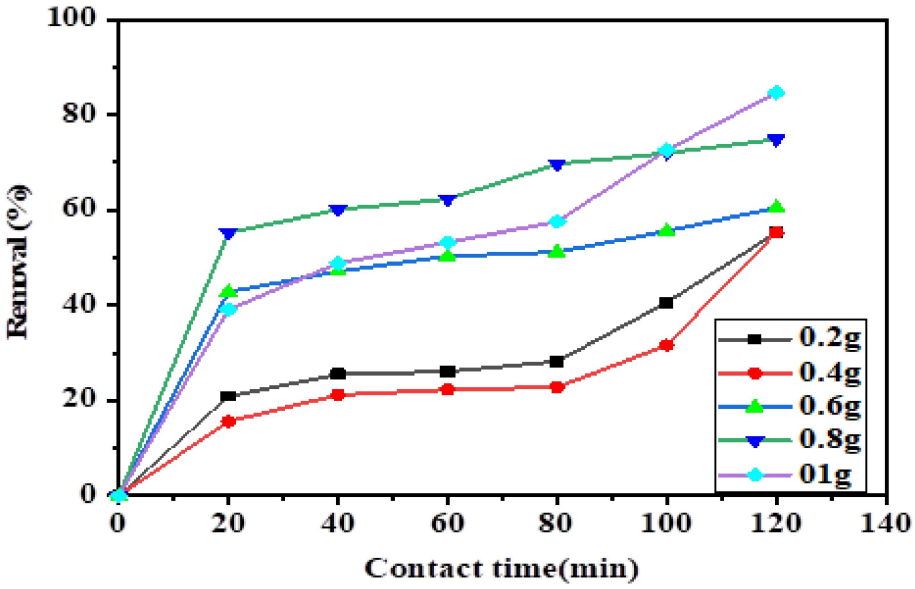

Figure 10. The effect of adsorbent dose on the removal of MB dye from wastewater effluent

Re-usability of Adsorbent

Fig. 11, represent the re-usability of Ni-CuO/ZB NC. It shows significant catalysts stability for efficient adsorption in the five cycles (99.04%, 94.28%, 92.05%, 90.10% and 84.65% respectively) taking 110 ppm concentration of Ni-CuO/ZB NC, 1.00 g adsorbent dose, at pH 12 and adsorption time of 120 min. A previous study using a different adsorbent (DSAC) reported its re-usability for phenol removal over eight cycles. The results showed good performance with removal efficiencies exceeding 96% in the initial cycles, but gradually decreasing with further use (96.12, 94.14, 91.01, 87.65, and 86.10 in the 1st, 2nd, 3rd, 4th and 5th cycles, respectively). This result is more comparable with the current finding and the decrease in adsorption capacity is likely due to the occupation of active sites on the adsorbent by pollutants over multiple cycles (Miri *et al.*, 2016). In the current study, Ni-CuO/ZB NC achieved an impressive adsorption performance of 99% under optimal conditions (110 ppm concentration of dye, 1.00 g of adsorbent dose, pH 12, and 120 min adsorption time). The promise of this technique lies in its reusability, stability, and high pollutant removal efficiency compared to existing methods (as shown in Appendix 1). For instance, a previous study by Tibebu *et al.* (2023) synthesized Ag-CdO/PANI NC for removing BPB dye from wastewater under ultraviolet-visible light irradiation while the effective treatment recorded 98%, this method requires light exposure. Another study by Girmaye *et al*. (2024) developed Ni-TiO_2/PANI NC for removing MG dye using photo-catalysis. This method achieved 99% degradation at optimized conditions, but it also has limitations such as generation of secondary pollutant. In this study, Ni-CuO/ZB NC offers a compelling alternative. It achieves comparable removal efficiency without the need for light or specific operating conditions beyond initial optimization. In general, this study provided a promising nanosorbent derived from agro-waste materials for wastewater pollutant adsorption and anticipated to offer a significant contribution to future environmental management strategies due to its potential for sustainability and effectiveness (Asefa *et al.*, 2024).

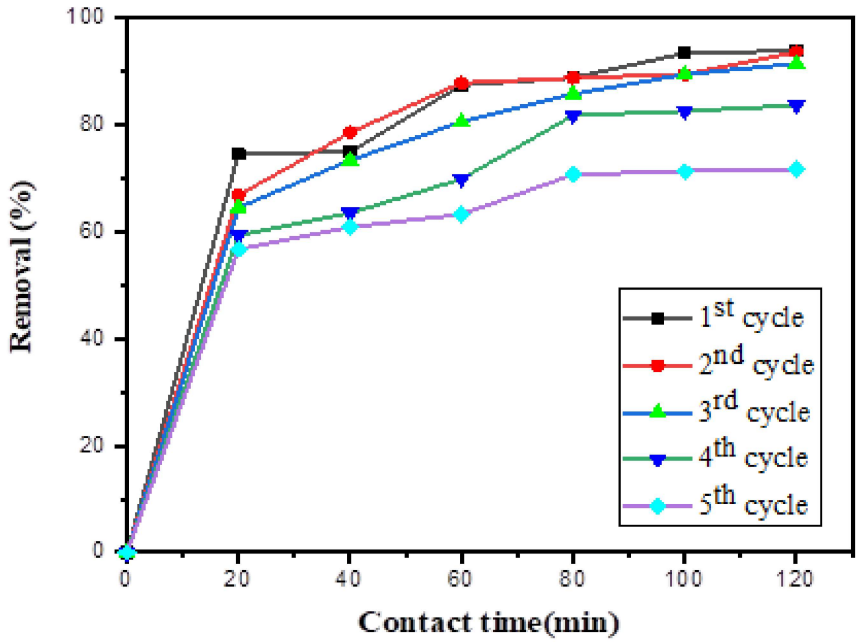

Figure 11.The re-usability of the adsorbent at optimum conditions for five consecutive cycles

Adsorption Isotherm

Langmuir adsorption isotherm: Fig. 12(a) shows the results of a Langmuir adsorption isotherm experiment, where MB molecules interact with the surface of the Ni-CuO/ZB NC adsorbent. The Langmuir isotherm model is often used to analyze the single-layer type of adsorption process. A key parameter in the Langmuir isotherm is the separation factor (R_L), calculated using Eq. 5. In the current study, the R_L value for MB adsorption was 0.0018, indicates a favorable adsorption (Kalaba *et al.*, 2022). Furthermore, the experiment yielded a high correlation coefficient (R^2) of 0.988 using non-linear model. This strong correlation supports the Langmuir isotherm model, suggesting that MB molecules form a single layer on the Ni-CuO/ZB NC adsorbent surface (Mohebali *et al.*, 2018).

Freundlich adsorption isotherm: Fig. 12(b) illustrates the Freundlich adsorption isotherm for MB on Ni-CuO/ZB NC. This isotherm model was used to analyze the favorability of the adsorption process. Using Eq. 6, the calculated value of 1/n was 0.4307, indicates that the MB is favorably adsorbed to Ni-CuO/ZB NC surface as its value fall between 0 and 1 suggesting favorable adsorption. The high correlation coefficient (R^2 = 0.991) from non-linear equation implies that the Freundlich isotherm provides a superior fit for describing MB adsorption at adsorbent compared to the Langmuir model since Freundlich adsorption model accounts for the heterogeneous surfaces with varying binding site affinities which agree with the finding of in particular the adsorption of MB dye on the semiconductor nanoparticles (Kalam *et al.*, 2021). As it was suggested by, Ni-CuO/ZB NC likely possesses a range of adsorption sites with different binding strengths for MB molecules so that it provided a successful adsorption of MB from wastewater sample (Arunkumar *et al.*, 2014).

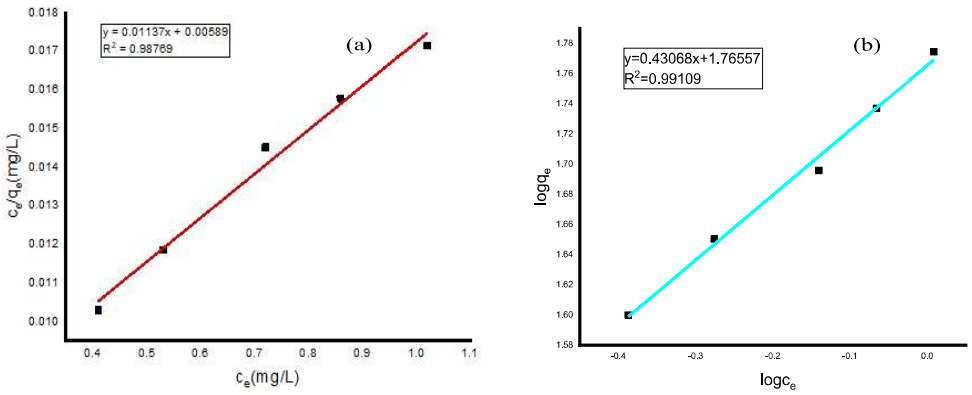

Figure 12. Adsorption model (a) Langmuir isotherm, (b) Freundlich isotherm for Ni-CuO/ZB NC

Adsorption Kinetic

Pseudo first-order kinetic model: Fig. 13(a), analyzes how MB adsorption onto the Ni-CuO/ZB NC surface follows a pseudo-first-order kinetic model. This model is well-suited for the studied adsorption timeframe and suggests that the interaction between MB and the NC primarily involves physisorption (Velusamy *et al.*, 2021). The key parameters which is the correlation coefficient (R^2 = 0.98189) is high value suggesting a strong correlation between the model and the experimental data where as an equilibrium adsorption capacity (q_e = 38.078 mg/g) represents the maximum amount of MB that can be adsorbed per unit mass of the NC under the studied conditions.

Pseudo second-order kinetic model: Figure 13(b), explores the kinetics of MB adsorption onto the Ni-CuO/ZB NC surface using the pseudo-second-order kinetic model. The analysis yielded the rate constant (k_2), equilibrium capacity (qe), and correlation coefficient (R^2). This suggests a slower removal rate at higher dye concentrations which attributed to the reduced diffusion of dye molecules as they encounter more occupied adsorption sites on the NC surface, becoming even more pronounced at high MB concentrations. The equilibrium adsorption capacity (q_e = 41.964 mg/g) and adsorption rate constant (k_2 = 0.0073). The fitting of the data to the pseudo-second-order model resulted in a high R^2 (0.99747), indicating a better fit compared to the pseudo-first-order model. This implies that the adsorption process likely follows a chemisorption mechanism, where valence forces through electron sharing between the NC and MB molecules govern the rate-limiting step (Abd El-Latif *et al.*, 2010).

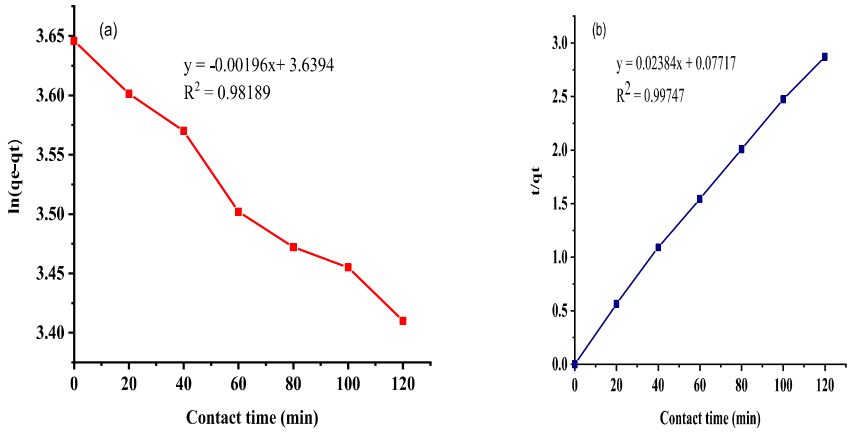

Figure 13. Adsorption Kinetics (a) Pseudo first-order model, (b) Pseudo second-order model

Adsorption Mechanism

The current study reveals the energy band gap (Eg) and particle size has decreased upon surface modification by ZB suggests an enhanced light absorption by Ni-CuO/ZB NC. This aligns with established principles where smaller particle size and lower Eg values typically improve light absorption efficiency. The investigation identified Ni-CuO/ZB NC is one of the most efficient adsorbent, achieving a remarkable 99.03% removal of MB dye under optimized conditions including adsorbate concentration of 110 ppm, pH 12, adsorbent dosage of 1.0 g and adsorption contact time of 120 min. The adsorption kinetic and isotherm model suggest that the adsorption process follows a pseudo-second-order kinetic (R^2 = 0.99), indicating chemisorption as the rate-limiting step. Additionally, the Freundlich isotherm model provides the best fit, implying a heterogeneous adsorption process with multilayer formation on the Ni-CuO/ZB NC surface {Modwi, 2018 #65}. In this work, the exceptional removal efficiency observed at the stated conditions confirmed that Ni-CuO/ZB NC surface exhibits a stronger adsorption capacity for MB dye in an alkaline (anionic) environment which creates a favorable electrostatic interaction toward cationic pollutants. Conversely, in acidic environment (lower pH), it likely leads to a positively charged adsorbent surface, repelling the cationic MB molecules and resulting in a lower adsorption capacity. Therefore, this adsorption process involves the formation of multilayers on the Ni-CuO/ZB NC surface, accompanied by chemisorption as the dominant mechanism.

Conclusion

Water pollution is a global issue that affects both human health and the aquatic habitat. This study aims to create CuO, Ni-CuO, Ni-CuO/activated carbon (AC), and Ni-CuO/zeamays bark (ZB) NCs for the removal of MB from industrial wastewater. The prepared nanomaterials were characterized using FT-IR, SEM, XRD, and UV-Vis analytical tools. FTIR spectra indicated the presence of OH and CO functional groups, enhancing adsorption potential. SEM revealed a porous, hair-like morphology in Ni-CuO nanocomposites. XRD analysis confirmed the formation of a monoclinic CuO phase, with a reduction in crystal size from 34.26 nm (CuO) to 18.06 nm (Ni-CuO/ZB). UV-Vis analysis showed a bandgap reduction from 3.22 eV (CuO) to 2.10 eV (Ni-CuO/AC) and 1.75 eV (Ni-CuO/ZB). The removal of MB exhibited that Ni-CuO/ZB achieved the highest removal efficiency of 99.03% under optimized conditions: 110 ppm dye concentration, pH 12, 1.0 g adsorbent dosage, and 120 minutes contact time. The adsorption process conformed to the Freundlich isotherm model

and pseudo-second-order kinetics (R^2 = 0.99), indicating multilayer adsorption and a chemisorption mechanism. Overall, the Ni-CuO/ZB nanocomposite demonstrated superior performance, making it a cost-effective and sustainable candidate for industrial wastewater treatment.

Data Availability Statement

All necessary data have incorporated within the manuscript and available whenever requested.

Statement of Conflict Of Interests

The authors declare that they have no known competing financial interests or personal relationships that could have appeared to influence the work reported in this paper.

References

Abd El-Latif, M., Ibrahim, A. M. and El-Kady, M. 2010. Adsorption equilibrium, kinetics and thermodynamics of methylene blue from aqueous solutions using biopolymer oak sawdust composite. *Journal of American science*, *6*(6), 267–283.

Al-Amri, S., Shahnawaze Ansari, M., Rafique, S., Aldhahri, M., Rahimuddin, S., Azam, A. and Memic, A. 2015. Ni doped CuO nanoparticles: structural and optical characterizations. *Current Nanoscience*, *11*(2), 191–197.

Al Ani, M., and Al Amri, M. 2015. The determinants of capital structure: an empirical study of Omani listed industrial companies. *Business: Theory and Practice*, *16*(2), 159–167.

Alemu, T., Merga, L. B., Amente, A. and Asefa, G. 2024. Treatment of wastewater dye using Ag–CdO-based nanocomposites surface modified with polyaniline. *Applied Nanoscience*, *14*(1), 177–189.

Alemu, T., Taye, G., Asefa, G. and Merga, L. B. 2022. Surface modification of Ag–CdO with polyaniline for the treatment of 3′, 3 ″, 5′, 5 ″-tetrabromophenolsulfonphthalein (BPB) under UV-visible light irradiation. *Heliyon*, *8*(11).

Andreucci, M., Solomon, R. and Tasanarong, A. 2014. Side effects of radiographic contrast media: pathogenesis, risk factors, and prevention. *BioMed research international*, *2014*(1), 741018.

Arunkumar, C., Perumal, R., Lakshmi, N. and Arunkumar, J. 2014. Use of corn cob as low cost adsorbent for the removal of nickel (II) from aqueous solution. *International Journal of Advanced Biotechnology and Research*, *5*(3), 325–330.

Asefa, G., Negussa, D., Lemessa, G. and Alemu, T. 2024. The study of photocatalytic degradation kinetics and mechanism of malachite green dye on Ni–TiO2 surface modified with polyaniline. *Journal of Nanomaterials*, *2024*(1), 5259089.

Ayawei, N., Ebelegi, A. N., and Wankasi, D. (2017). Modelling and interpretation of adsorption isotherms. *Journal of chemistry*, *2017*(1), 3039817.

Azari, A., Malakoutian, M., Yaghmaeain, K., Jaafarzadeh, N., Shariatifar, N., Mohammadi, G. and Kamani, H. (2022). Magnetic NH_2-MIL-101 (Al)/Chitosan nanocomposite as a novel adsorbent for the removal of azithromycin: modeling and process optimization. *Scientific Reports*, *12*(1), 18990.

Bedmohata, M., Chaudhari, A., Singh, S. and Choudhary, M. 2015. Adsorption capacity of activated carbon prepared by chemical activation of lignin for the removal of methylene blue dye. *International Journal of Advanced Research in Chemical Science (IJARCS)*, *2*(8), 1–13.

Chakraborty, T., Islam, M., Zaman, S., Kabir, A. and Ghosh, G. 2020. Jute (Corchorus olitorius) stick charcoal as a low-cost adsorbent for the removal of methylene blue dye from aqueous solution. *SN Applied Sciences*, *2*(4), 765.

Chandrasekar, M., Subash, M., Logambal, S., Udhayakumar, G., Uthrakumar, R., Inmozhi, C., Al-Onazi, W. A., Al-Mohaimeed, A. M., Chen, T.-W. and Kanimozhi, K. 2022) Synthesis and characterization studies of pure and Ni doped CuO nanoparticles by

hydrothermal method. *Journal of King Saud University-Science*, *34*(3), 101831.

Chesman, A. S., Duffy, N. W., Peacock, S., Waddington, L., Webster, N. A. and Jasieniak, J. J. (2013). Non-injection synthesis of Cu 2 ZnSnS 4 nanocrystals using a binary precursor and ligand approach. *RSC advances*, *3*(4), 1017–1020.

Chowdhury, A., Kumari, S., Khan, A. A., Chandra, M. R. and Hussain, S. 2021. Activated carbon loaded with Ni-Co-S nanoparticle for superior adsorption capacity of antibiotics and dye from wastewater: kinetics and isotherms. *Colloids and Surfaces A: Physicochemical and Engineering Aspects*, *611*, 125868.

Dwivedi, L. M., Shukla, N., Baranwal, K., Gupta, S., Siddique, S. and Singh, V. 2021. Gum Acacia modified Ni doped CuO nanoparticles: an excellent antibacterial material. *Journal of Cluster Science*, *32*, 209–219.

El Malti, W., Koteich, S. and Hijazi, A. 2024. Utilizing Chamaerops humilis in removing methylene blue dye from water: an effective approach. *RSC advances*, *14*(33), 24196–24206.

Ersali, S., Hadadi, V., Moradi, O. and Fakhri, A. 2013. Pseudo-second-order kinetic equations for modeling adsorption systems for removal of ammonium ions using multi-walled carbon nanotube. *Fullerenes, Nanotubes and Carbon Nanostructures*(just-accepted).

Fallah Jokandan, S., Esrafili, A., Yousefzadeh, S., Ahmadi, E., Azari, A., Mokhtari, S. A., and Gholami, M. 2018. Optimization of advanced oxidation process based on persulfate ($Uv/Na_2S_2O_8/Fe^{2+}$) for phthalic acid removal from aqueous solutions with response surface methodology. *Journal of Babol University of Medical Sciences*, *20*(2), 13-21.

Fu, L., Ren, Z., Si, W., Ma, Q., Huang, W., Liao, K., Huang, Z., Wang, Y., Li, J. and Xu, P. 2022. Research progress on CO_2 capture and utilization technology.

Gharibzadeh, F., Kalantary, R. R., Esrafili, A., Ravanipour, M., and Azari, A. 2019. Desorption kinetics and isotherms of phenanthrene from contaminated soil. *Journal of Environmental Health Science and Engineering*, *Journal of CO_2 Utilization*, *17*(1), 171-181.

Gomathi, S., Nachiyar, G. V. and Nandini, P. 2016. Effect of Surfactant on the Structural and Optical Properties of CuO Nanoparticles. *International Journal of Scientific Reseach*, *5*, 339–341.

Hasanzadeh, M., Ghaedrahmat, Z., Kayedi, N., Fard, N. J. H., Azari, A. and Afsharizadeh, M. 2023. Persulfate-assisted heterogeneous photocatalytic degradation of furfural from aqueous solutions using TiO2–ZnO/biochar composite. *Heliyon*, *9*(11).

Hii, H. T. 2021. Adsorption isotherm and kinetic models for removal of methyl orange and remazol brilliant blue r by coconut shell activated carbon. *Tropical Aquatic and Soil Pollution*, *1*(1), 1–10.

Hosseinzehi,K. H M., Ghayebzadeh, M., Azari, A., Ashrafi, S. D., and Abdipour, H. 2024. Degradation of reactive red 198 dye from aqueous solutions by combined technology advanced sonofenton with zero valent iron: Characteristics/effect of parameters/kinetic tudies. *Heliyon*, *10*(1).

Igwegbe, C. A., Oba, S. N., Aniagor, C. O., Adeniyi, A. G. and Ighalo, J. O. 2021. Adsorption of ciprofloxacin from water: a comprehensive review. *Journal of Industrial and Engineering Chemistry*, *93*, 57–77.

Islam, M. M., Aidid, A. R., Mohshin, J. N., Mondal, H., Ganguli, S. and Chakraborty, A. K. 2025. A critical review on textile dye-containing wastewater: Ecotoxicity, health risks, and remediation strategies for environmental safety. *Cleaner Chemical Engineering*, 100165.

Juma, A. O., Arbab, E. A., Muiva, C. M., Lepodise, L. M. and Mola, G. T. 2017. Synthesis and characterization of CuO-NiO-ZnO mixed metal oxide nanocomposite. *Journal of alloys and compounds*, *723*, 866–872.

Kalaba, G., Nyirenda, J. and Munyati, O. 2022. Characterisation of activated carbons for removal of organic and heavy metal pollutants from water in resource limited

countries. *Desalination and Water Treatment*, *261*, 224–233.

Kalam, S., Abu-Khamsin, S. A., Kamal, M. S. and Patil, S. 2021. Surfactant adsorption isotherms: A review. *ACS omega*, *6*(48), 32342–32348.

Kamani, H., Hosseinzehi, M., Ghayebzadeh, M., Azari, A., Ashrafi, S. D. and Abdipour, H. 2024. Degradation of reactive red 198 dye from aqueous solutions by combined technology advanced sonofenton with zero valent iron: Characteristics/effect of parameters/kinetic studies. *Heliyon*, *10*(1).

Khan, S., Pandian, J. D., Lal, D. V., Rugel, M. R., Brunthaler, A., Menten, K. M., Wyrowski, F., Medina, S.-N., Dzib, S. and Nguyen, H. 2022. A multiwavelength study of the W33 Main ultracompact HII region. *Astronomy and Astrophysics*, *664*, A140.

Lakkaboyana, S. K., Khantong, S., Asmel, N. K., Yuzir, A. and Wan Yaacob, W. Z. 2019. Synthesis of copper oxide nanowires-activated carbon (AC@ CuO-NWs) and applied for removal methylene blue from aqueous solution: kinetics, isotherms, and thermodynamics. *Journal of Inorganic and Organometallic Polymers and Materials*, *29*, 1658–1668.

Luong, H. V. T., Le, T. P., Le, T. L. T., Dang, H. G. and Tran, T. B. Q. (2024). A graphene oxide based composite granule for methylene blue separation from aqueous solution: Adsorption, kinetics and thermodynamic studies. *Heliyon*, *10*(7).

Matandabuzo, M. 2016. Remediation of metal ions in aqueous solution using activated carbon from Zea may stem.

Medhat, A., El-Maghrabi, H. H., Abdelghany, A., Menem, N. M. A., Raynaud, P., Moustafa, Y. M., Elsayed, M. A. and Nada, A. A. 2021. Efficiently activated carbons from corn cob for methylene blue adsorption. *Applied Surface Science Advances*, *3*, 100037.

Miri, M., Shendi, M. R. A., Ghaffari, H. R., Aval, H. E., Ahmadi, E., Taban, E., Gholizadeh, A., Aval, M. Y., Mohammadi, A. and Azari, A. 2016. Investigation of outdoor BTEX: Concentration, variations, sources, spatial distribution, and risk assessment. *Chemosphere*, *163*, 601–609.

Mohebali, M., Moradi-Asl, E. and Rassi, Y. 2018. Geographic distribution and spatial analysis of Leishmania infantum infection in domestic and wild animal reservoir hosts of zoonotic visceral leishmaniasis in Iran: A systematic review. *Journal of vector borne diseases*, *55*(3), 173–183.

Morsy, A., Rashad, M., Shaalan, N. and Abdel-Rahim, M. 2019. Influence of Ni doping on CuO nanoparticles synthesized by rapid solid reaction method. *Micro and Nanosystems*, *11*(2), 109–114.

Mousavi, S. A., Mahmoudi, A., Amiri, S., Darvishi, P. and Noori, E. 2022. Methylene blue removal using grape leaves waste: optimization and modeling. *Applied Water Science*, *12*(5), 112.

Opeolu, B. O. (2009). Utilization of maize (Zea mays) cob as an adsorbent for lead (II) removal from aqueous solutions and industrial effluents. *African journal of Biotechnology*, *8*(8).

Rabiee, F., Sarkhosh, M., Azizi, S., Jahantigh, A., Hashemi, S. Y., Baziar, M., and Azari, A. 2024. The superior decomposition of 2, 4-Dinitrophenol under ultrasound-assisted Fe_3O_4@TiO_2 magnetic nanocomposite: process modeling and optimization, Effect of various oxidants and Degradation pathway studies. *International Journal of Environmental Analytical Chemistry*, *104*(6), 1243-1265.

Rashed, M. N., Eltaher, M. and Abdou, A. 2017. Adsorption and photocatalysis for methyl orange and Cd removal from wastewater using TiO_2/sewage sludge-based activated carbon nanocomposites. *Royal society open science*, *4*(12), 170834.

Raut, E. R., Thakur, M. A. B. and Chaudhari, A. R. 2021. A review on activated carbon preparation from natural and eco-friendly raw materials. AIP Conference Proceedings,

Robertson, I., Holzer, L., Prestat, M., Münch, B. and Graule, T. 2010. Effects of particle and pore sizes, surface area and porosity

on the performance of LSC cathodes. Proc. 9th European Fuel Cell Forum,

Salih, S. J., Kareem, A. S. A. and Anwer, S. S. 2022. Adsorption of anionic dyes from textile wastewater utilizing raw corncob. *Heliyon*, *8*(8).

Satari, C., Sidqi, R. S., Putra, F., Putri, S. and Nandiyanto, A. 2021. Literature review: synthesis of CuO (Copper Oxide) nanoparticles for thermal energy storage. *Int J Energetica*, *6*, 21–34.

Shah, Z., Hassan, S., Shaheen, K., Khan, S. A., Gul, T., Anwar, Y., Al-Shaeri, M. A., Khan, M., Khan, R. and Haleem, M. A. 2020. Synthesis of AgNPs coated with secondary metabolites of Acacia nilotica: An efficient antimicrobial and detoxification agent for environmental toxic organic pollutants. *Materials Science and Engineering: C*, *111*, 110829.

Shahmohammadi-Kalalagh, S., Babazadeh, H., Nazemi, A. and Manshouri, M. 2011. Isotherm and kinetic studies on adsorption of Pb, Zn and Cu by kaolinite. *Caspian Journal of Environmental Sciences*, *9*(2), 243–255.

Sharma, G., Sharma, S., Kumar, A., Lai, C. W., Naushad, M., Shehnaz, Iqbal, J. and Stadler, F. J. 2022. Activated carbon as superadsorbent and sustainable material for diverse applications. *Adsorption Science and Technology*, *2022*, 4184809.

Sharma, P. and Singh, S. P. 2021. Pollutants characterization and toxicity assessment of pulp and paper industry sludge for safe environmental disposal. In *Emerging Treatment Technologies for Waste Management* (pp. 207–223). Springer.

Sravanthi, M., Muni Kumar, D., Usha, B., Ravichandra, M., Mahendra Rao, M., Hemalatha, K. and Ravichandra, M. 2016. Biological synthesis and characterization of copper oxide nanoparticles using Antigonon leptopus leaf extract and their antibacterial activity. *Int. J. Adv. Res*, *4*(8), 589–602.

Sukumar, S., Rudrasenan, A. and Padmanabhan Nambiar, D. 2020. Green-synthesized rice-shaped copper oxide nanoparticles using Caesalpinia bonducella seed extract and their applications. *ACS omega*, *5*(2), 1040–1051.

Suryowati, T. 2024. Biochemical aspects of cell staining. *Asian Journal of Research in Biochemistry*, *14*(3), 61–71.

Suteu, D., Malutan, T. and Bilba, D. 2011. Agricultural waste corn cob as a sorbent for removing reactive dye orange 16: equilibrium and kinetic study. *Cellulose chemistry and technology*, *45*(5), 413.

Tigrine, Z., Benhabiles, O., Merabti, L., Chekir, N., Mellal, M., Aoudj, S., Abdeslam, N. A., Tassalit, D., Lebouachera, S. E. I. and Drouiche, N. 2024. Sustainable Activated Carbon from Agricultural Waste: A Study on Adsorption Efficiency for Humic Acid and Methyl Orange Dyes. *Sustainability*, *16*(21), 9308.

Veisi, F., Zazouli, M. A., Ebrahimzadeh, M. A., Charati, J. Y. and Dezfoli, A. S. 2016. Photocatalytic degradation of furfural in aqueous solution by N-doped titanium dioxide nanoparticles. *Environmental Science and Pollution Research*, *23*, 21846–21860.

Velusamy, S., Roy, A., Sundaram, S. and Kumar Mallick, T. 2021. A review on heavy metal ions and containing dyes removal through graphene oxide-based adsorption strategies for textile wastewater treatment. *The Chemical Record*, *21*(7), 1570–1610.

Xie, L. S., Skorupskii, G. and Dinca, M. 2020. Electrically conductive metal–organic frameworks. *Chemical reviews*, *120*(16), 8536–8580.

Yang, H. and Yang, J. 2018. Photocatalytic degradation of rhodamine B catalyzed by TiO_2 films on a capillary column. *RSC advances*, *8*(22), 11921–11929.

Appendix

Summary of previous research report using various pollutant removal methods with key parameters, adsorbents, adsorbent's and findings are highlighted as follows:

Adsorbent used	Focus of the study	Method employed	Target pollutant	Optimum condition and key finding	References
Zero-valent iron (NZVI) NP	The zero-valent iron (NZVI) NPs for the decomposition of Reactive Red 198.	Advanced Sono-Nano-Fenton hybrid method	Reactive Red 198	Degradation efficiency was 97 % achieved by Sono-Nano Fenton process in 60 min and the process follows pseudo-first-order kinetics and the Langmuir-Hinshelwood model.	Hossein K. et al., 2024
TiO_2–ZnO/biochar activator of persulfate	TiO_2–ZnO/biochar NCs as activator of persulfate (PS) for degradation of furfural	Sol-gel method	furfural	Efficiency: 96 % of furfural at pH = 3, catalyst dosage = 1 g/L, persulfate concentration = 1.2 mM, and furfural concentration = 10 mg/L) within 15 min. The experimental data fitted well with the first-order kinetic model	Hasanzadeh, M. et al., 2023
Na_2S_2O/Fe^{2+})	Conducted to Optimize ($UV/Na_2S_2O_8/Fe^{2+}$) process for phthalic acid removal	Response surface method	Phthalic Acid	Removal efficiency: 98% at pH= 11, reaction time=60 min, Fe^{2+} concentration=0.15 mmol/L, persulfate concentration = 0.3 mmol/L and phthalic acid =5 mg. The phthalic acid removal followed by first-order kinetic.	Fallah J. *et al.,* 2018
Desorption from soil	Evaluating the desorption kinetics of phenanthrene	The nonionic surfactant	(PAHs)	The desorption was well described by pseudo-second-order model and fitted well by Freundlich isotherm models	Gharibzadeh F. et. al., 2019
MIL/Cs@Fe_3O_4 NCs	magnetic NH_2-MIL-101(Al)/chitosan NCs for the adsorption of azithromycin (AZT)	Microwave method	Azithromycin (AZT)	At pH= 7.992, adsorbent dose=0.279 g/L, time= 64.256 min and AZT =10.107 mg/L the adsorption efficiency and AZT adsorption capacity were 98.362 ± 3.24% and 238.553 mg/g, respectively. The data well fitted the Langmuir isotherm and Pseudo-second-order kinetics.	Azari, A. et al., 2022
Fe_3O_4@TiO_2 magnetic nanocomposite	Ultrasound-assisted Fe_3O_4@TiO_2 for catalytic oxidation of 2, 4-Dinitrophenol.	RSM-based CCD approach	2,4-Dinitrophenol	Over 91.45% of DNP were removed by Fe_3O_4@TiO_2 /US system (FTU) under optimum conditions within 30 min	Rabiee, F. et. al., 2024
Ni-CuO NCs treated with AC prepared from ZB	Designed for removal of methylene blue (MB) dye from wastewater	Adsorption	Methylene Blue Removal	Ni-CuO/ZB NC showed optimal adsorption at 110 ppm, pH 12, 0.8 g dosage, and 120 min contact time, achieving 99.03% removal efficiency. The process followed Freundlich isotherm and pseudo-second-order kinetics.	This study